Atmospheric Icing of Transmission Line Conductor Bundles

T. Wagner[*,1], *U. Peil*[2]
[1] *International Graduate School of Risk Management of Natural and Civilization Hazards on Buildings and Infrastructure,* [2] *Institut of Steel Structures, Technical University Braunschweig*
[*] *Corresponding author: Beethoven Straße 51, 38106 Braunschweig, Germany, t.wagner@tu-bs.de*

Abstract: Hazardous for the transmission lines is not only the static ice load, but also the aerodynamic instability of iced cables. It can lead to large amplitude oscillations at low frequencies and also twisting due to asymmetrical iced cables may increase the fatigue rate. In extreme events atmospheric icing can cause severe damages on towers and power lines resulting in extensive electricity breakdown. Therefore the shape and the density of the ice forming on the cable are of major interest in investigating the risk of failure. This is the first part of a simulation scheme going to be developed in order so investigate whole hazard scenarios for transmission lines under a variety of meteorological condition and conductor bundle characteristics. The simulation scheme is manly inspired by the aerospace engineering, since significant attention has been paid to ice accumulation in aircraft design.

Keywords: transmission lines icing, particle tracing, CFD, domain tracking

1 Introduction

Atmospheric icing occurs when freezing raindrops, super cooled cloud droplets or snow flakes hit a surface. In combination with wind, this phenomenon can causes significant damage to electric power transmission networks. The damages occur as a large number of singly failed structures as well as by major winter storm events [12, 18]. Due to oscillations with large amplitude at low frequencies and also twisting due to asymmetrical iced cables may increase the fatigue rate. In extreme events atmospheric icing can cause severe damages on towers and power lines [2, 8, 10, 16]. Therefore the shape and the density of the ice forming on the cable are of major interest in investigating the risk of failure. Modern societies are increasingly vulnerable to blackouts with the growing demand of energy and increasing capacity utilisation. The devastating power of winter storms arise in 1998 in Canada and to a much smaller extent in 2005 in Germany. Leaving many people without electricity for weeks and causing significant monetary damages [7, 11, 20].

The simulation of atmospheric icing requires both, a computation of the mass flux of icing particles as well as a determination of the ice growing conditions. The last is obviously governed by the heat balance on the ice surface. It influences accretion mass and furthermore the evolving ice density strongly. From an engineering point of view there are three major types of ice, leading to significant loads on structures. Two of them, glaze ice and wet snow, are dedicated to wet growing regime, where the heat balance on the ice surface is very important. Based on the mass flux of icing particles it defines the evolution of the ice shape and density. In case of rime ice, which forms in dry growing conditions, the heat transfer in the system can be neglected. Because the latent heat of the droplets released in the freezing process is dissipated without changing the state of the ice and the surface conditions from dry to wet. The present work is focusing on the mass flux of icing particles and the evolution of the ice front and therefore on the formation of rime ice. Based on flow field calculation the trajectories of the impinging precipitation droplets are determined. Their characteristics have a major influence on the shape and to a smaller extent on the density of ice evolution. Already existing numerical cable icing models are restricted to a single cable due to the assumptions made regarding the flow field calculation [6, 9, 13, 15, 16, 19]. Therefore a simulation scheme is presented allowing for particle motion based on the stream occurring

around conductor bundles. The calculation of the 2D flow field is based on the incompressible and isothermal Navier-Stokes equation in conjunction with the k-ϵ-turbulence model. The fluid domain is discretized in a combination of a mapped boundary layer mesh in vicinity of the bodies in the stream and with a free mesh consisting of triangles in the remaining domain. In order to describe the droplet motion in the fluid the Lagrangian approach is used, meaning that individual particle trajectories are modelled. It is used even though it is not providing information about the particle density in the flow field. Presuming, there will be a low particle concentration in the flow any effect of the particles on the fluid flow is neglected. Hence, decoupling of the fluid dynamic calculation and the droplet motion description by the Lagrangian method is justified.

2 Fluid Dynamics

The 2D flow field around a conductor bundle is calculated with the incompressible and isothermal Navier-Stokes equation, which is solved by Reynolds-Average-Navier-Stokes (RANS) solver [4]. In the scope of feasible wind velocities assuming a constant fluid density is reasonable, as well as neglecting the heat emission of the cables in the flow calculation. Therefore the incompressible and isothermal Navier-Stokes is applicable. Hence, the conservation of mass becomes

$$\nabla u = 0 \tag{1}$$

where u is the velocity vector. Emanate from considering a Newton fluid and together with the Stokes assumption the stress tensor becomes

$$\tau = \eta(\nabla u + (\nabla u)^T) \tag{2}$$

where η is the dynamic viscosity. The conservation of momentum is than

$$\begin{aligned} \rho\frac{\partial u}{\partial t} + (\rho u\nabla)u = \\ -\nabla p + \nabla\Big(\eta\left(\nabla u + (\nabla u)^T\right)\Big) + F \end{aligned} \tag{3}$$

with the fluid density ρ, the pressure p and the force vector F acting on the body. The conservation of energy is expressed in terms of temperature, which is in our case constant in the whole fluid domain.

The closure problem of the RANS equations is solved by a k-ϵ-turbulence model modelling the turbulent viscosity. It introduces the turbulent kinetic energy k and the dissipation rate of turbulence ϵ as independent variables. The turbulent viscosity is than determined by

$$\eta_T = \rho C_\mu \frac{k^2}{\epsilon} \tag{4}$$

The turbulent kinetic energy k is derived by the Reynold stresses, which are expressed by

$$\begin{aligned} \rho\frac{\partial k}{\partial t} - \nabla\Big(\Big(\eta + \frac{\eta_T}{\sigma_k}\Big)\nabla k\Big) + \rho u\nabla k = \\ \frac{1}{2}\eta_T\left(\nabla u + (\nabla u)^T\right)^2 - \rho\epsilon \end{aligned} \tag{5}$$

where $u[\frac{m}{s}]$ is the average velocity field. The equation is than defined as

$$\begin{aligned} \rho\frac{\partial \epsilon}{\partial t} - \nabla\Big(\Big(\eta + \frac{\eta_T}{\sigma_\epsilon}\Big)\nabla \epsilon\Big) + \rho u\nabla \epsilon = \\ \frac{1}{2}C_{\epsilon 1}\frac{\epsilon}{k}\eta_T\left(\nabla u + (\nabla u)^T\right)^2 - \rho C_{\epsilon 2}\frac{\epsilon^2}{k} \end{aligned} \tag{6}$$

The used set of model constants is $C_\mu = 0.09$, $\sigma_k = 1.0$, $C_{\epsilon 1} = 1.44$, $C_{\epsilon 2} = 1.92$ and $\sigma_\epsilon = 1.3$, which are based on experiments published in [21].

An assumption made by this turbulence model is the equilibrium of turbulence in boundary layers and therefore the formation and dissipation of turbulences are equal. Since this is not always true, the spatial extension of recirculation zones is usually underestimated [5]. Another limitation of the model is the stagnation point anomaly, which is due to an overestimation of k in the stagnation flow regions. It causes a weak representation of the pressure distribution on the windward surfaces and especially behind the first corner [5]. The underestimation of the recirculation zone keeps the model on the save side. Because the impact of the bundle arrangement on particle flux and therefore on the accretion process of the cable in the wake will always be underestimated. The second assumption leading to imprecise pressure field has no impact on the ice formation itself, but it is a back draw in terms of galloping investigation and load estimations on the transmission line structure. But this problem can be addressed in separated CFD calculations focusing on these issues.

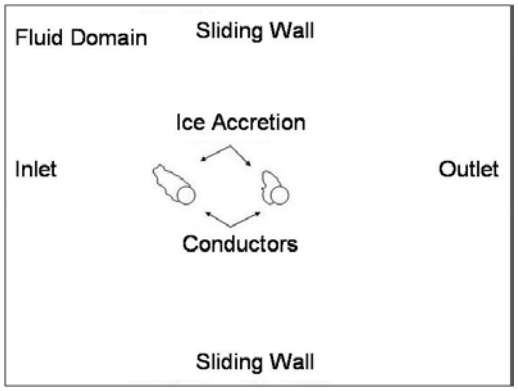

Figure 1: Schema of the model layout

2.1 Boundary Conditions

In order to reduce the influence of the model boundary the model is divided in a far and a near field. The near field is main fluid domain, enclosing the conductor bundle. Here the actual investigation takes place. It is surrounded by the far field, which gives the necessary distance between the model boundaries and the near field to eliminate any interference on the flow in the near field. The distance is greater than 50 times the maximum expected characteristic length of an iced conductor bundle in the stream.

The boundary condition at the inlet gives the ambient velocity u_a normal to the boundary.

$$u_0 = u_a \tag{7}$$

In addition constrains for k and ϵ are needed, which is done by means of the turbulence intensity I_T and the turbulence length scale L_T. The first describes the grade of turbulence and the second the eddy size which is not resolved in the model [3]. Giving the following equations

$$k = \frac{3}{2}(|u|I_T)^2 \tag{8}$$

$$\epsilon = C_\mu^{3/4}\frac{k^{3/2}}{L_T} \tag{9}$$

The outlet boundary sets the viscous stresses to be vanished in conjunction with Dirichlet Boundary condition for the pressure

$$\eta(\nabla u + (\nabla u)^T)\cdot n = 0 \tag{10}$$

$$p = p_0 \tag{11}$$

and

$$n\cdot\nabla k = 0 \tag{12}$$

$$n\cdot\nabla \epsilon = 0 \tag{13}$$

for k and ϵ.

In conjunction with the turbulence model the boundary conditions at walls are described via logarithmic wall functions [3]. It assumes a flow parallel to the wall in layer up to δ_w from the wall. The velocity parallel to the wall $u_\parallel$ is achieved by

$$\frac{u_\parallel}{u_\tau} = \frac{1}{\kappa} ln\left(\frac{\delta_w}{l^*}\right) + C^+ \tag{14}$$

with the friction velocity

$$u_\tau = \sqrt{\frac{\tau}{\rho}} \tag{15}$$

and the viscous length scale

$$l^* = \frac{\eta}{\rho u_\tau} \tag{16}$$

where the Kármán constant $\kappa = 0.42$ and the universal constant for smooth walls $C^+ = 5.5$. The layer dimension δ_w can be expressed in viscous dimension leading to

$$\delta_w^+ = \delta_w / l^* \tag{17}$$

where $\delta_w^+ = 100$ is set within the valid rang. The interrelationship between δ_w^+ and δ_w is be expressed by

$$\delta_w^+ = \frac{\rho C_\mu^{1/4} k^{1/2}\delta_w}{\eta} \tag{18}$$

For k and ϵ is than assumed that the production and dissipation of turbulences is equal in the computation offset of the wall.

$$n\cdot\nabla k = 0 \tag{19}$$

$$\epsilon = \frac{C_\mu^{3/4} k^{3/2}}{\kappa\delta_w} \tag{20}$$

This set of equations is applied on the ice and cable surfaces. The upper and lower boundary of the far field is modelled as sliding walls. Therefore the equation 14 is modified by

$$\frac{u_\parallel - u_w}{u_\tau} = \frac{1}{\kappa} ln\left(\frac{\delta_w}{l^*}\right) + C^+ \tag{21}$$

with the wall velocity

$$u_w = u_a \tag{22}$$

2.2 Mesh

The fluid domain is discretized in a combination of a mapped boundary layer mesh in vicinity of the bodies in the stream and with a free mesh consisting of triangles in the remaining domain. First the near field is meshed with a fine triangular mesh upon which a boundary layer mesh is added at the ice and cable surfaces. The far field is meshed with a very coarse triangular mesh to avoid any effects of the model boundary on the near field.

2.3 Solver

The stationary segregated solver is applied to calculate the fluid domain in combination with the linear system solver PARDISO [3]. The velocity components and the pressure are solved in the first group and the turbulent kinetic engergy and the turbulent dissipation rate are solved in the second group. THe final error estimate for both groups is smaller than 0.001. The standard settings are used except for the *damping*, which is set to be 0.1, and for the scaling type is set to *automatic*. As streamline diffusion method for both the turbulence model and the Navier-Stokes equation Galerkin Least-Square is used.

3 Particle Tracing

The Lagrangian approach is used to calculate the particle motion in the flow. It is used even though no information about the particle density in the flow field are providing. In contrast to that, the Eulerian approach describes the particles as a continuum, where the distribution of the particles is included by a particle density function. The advantage of the first method is that it can represent the intersection of droplet trajectories in the wake of bodies in the stream [22]. It is presumed, there will be a low particle concentration in the flow. Based on this assumption any effect of the particles on the fluid flow is neglected. Therefore decoupling of the fluid dynamic calculation and the droplet motion description by the Lagrangian method is justified. The particle motion is described by [3]

$$F = \pi r_p^2 \rho (\bar{u} - \bar{u}_p)^2 (1.84 (Re_p)^{-0.31} + 0.293 Re_p^{0.06})^{3.45} \quad (23)$$

where r_p is the droplet radius, $\bar{u}$ the fluid velocity, $\bar{u}_p$ droplet velocity and Re_p the droplet Reynolds number

$$Re_p = \frac{(|\bar{u} - \bar{u}_p| 2 r_p \rho)}{\eta} \quad (24)$$

The solver rewrites this second order ordinary differential equation (ODE) into a pair of coupled first order ODE. In each direction has one equation for the velocity and one for the location. This system is then solved by a pair of four and five order Runge-Kutta methods [3, 4]. In order to simulate the behaviour of natural precipitation it is not necessary to apply the whole droplet spectra. It is sufficient to model only the particle motion of a droplet with the medium volume diameter (MDV) and a predefined spacing [17]. It is presumed that the trajectories of those of particles provide sufficient information of the behaviour of whole droplet spectra.

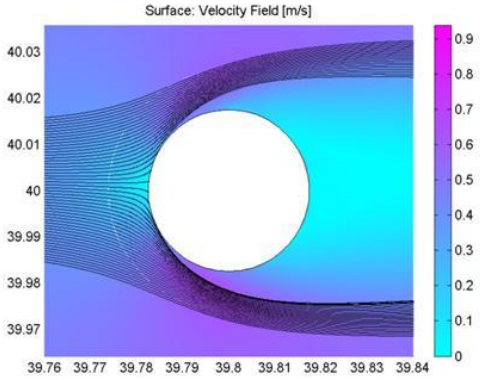

Figure 2: Droplet trajectories impinging on a cable with a wind velocity of $0.5 m/s$ and a medium volume diameter of $34 \mu m$

4 Ice Accretion Process

Once the end points of the particle trajectories are given the investigation of the ice evolution can start. First the end points of the trajectories are aligned with the fine discretized ice or cable surface. Those impact points are considered in the following procedure. Among the active points continues surfaces are defined and at each point the impact velocity and impact angle are defined. In order to leave the ice evolution unrestricted by the algorithm ice and cable sections are treated as one. Upon which

the new ice layer is formed along the sections with particle impact. The collection efficiency is the ratio of the flux density of those droplets sticking to the object to the flux density of all droplets hitting the object [17]. The difference arises from particles bouncing back from the surface. It is given by

$$\beta = \frac{A_0 \cos(\alpha)}{A_i} \tag{25}$$

where α is the impact angle. A_0 is the initial trajectory spacing in the undisturbed flow and A_i is the trajectory spacing when the particle impinging on the surface. The developing ice density in kilogram per cubic meter can be determined by empirical equations [1]

$$\rho_i = 110 \cdot R^{0.76} \qquad R \leq 10 \tag{26}$$

$$\rho_i = \frac{R}{R + 5.61} \cdot 10^3 \qquad 10 < R \leq 60 \tag{27}$$

$$\rho_i = 917 \qquad R > 60 \tag{28}$$

where R is the Macklin's Parameter [14].

$$R = \frac{MDV \cdot u_s}{2 \cdot T_s} \tag{29}$$

where MDV is the medium volume diameter, u_s the impact speed and T_s the surface temperature. In conjunction with the liquid water content (LCW) in the air the accretion density ratio is achieved

$$\chi = \frac{LCW}{\rho_i} \tag{30}$$

Than new coordinates offset of the new ice front is expressed in

$$e_i = u_0 \cdot \chi \cdot \beta \cdot t_{int} \tag{31}$$

where t_{int} is the time interval of ice evolution with unchanged flow field. These points are establishing the new ice front section. Finally the whole new surface is assembled from specific sections of new ice sections and the remaining ice and cable sections.

5 Domain Tracking

Not a trivial task is the domain assignment during the model assembling. It is nether known in advance where and in which shape the ice is formed nor if it is grown or shrinken with respect to the former time step. Therefore the domain numbering needs to be automatised to ensure continues calculation process. It is done by assembling different domain types successively. First the *FluidDomain*is analyzed in order to create the investigation space. Then the *CableDomain* and *IceDomain* are added in an individual analyze step. The subdomain and boundary indices are tracked by self implemented function. The output matrixes are *track_domains*used to assign the settings and boundary conditions of the fluid, cable and ice domain in the application modes.

```
% Investigation Space
[Fluid,st1,ct1]=geomcsg({g1,g2}, ...
           'ns',{'g1,'g2'}, ...
           'sf',{'g1+g2'}, ...
           'out',{'g','stx','ctx'});

% Inserting Cable Geometry
[Fluid,st2,ct2]=geomcsg({Fluid,Cabel}, ...
           'ns',{'Fluid','Cabel'}, ...
           'sf','Fluid-Cabel', ...
           'out',{'g','stx','ctx'});

% Inserting Ice Geometry
[Fluid,st3,ct3]=geomcsg({Fluid,Ice}, ...
           'ns',{'Fluid','Ice'}, ...
           'sf','Fluid-Ice', ...
           'out',{'g','stx','ctx'});

% Track Domains
[Fluid_st,Cable_st,Ice_st]= ...
            track_domains(st1,st2,st3);
[Fluid_ct,Cable_ct,Ice_ct]= ...
            track_domains(ct1,ct2,ct3);
```

This structure is not only beneficial incase of an unchanged space of investigation enclosing changing objected under investigation. But also in the scope of sensitivity analysis and optimisation problems. If a sensitivity analysis or an optimisation algorithm is not only applied on of physical model parameters, but also number or position of objects or rather domains is done.

6 Discussion

The fluid dynamic calculation faces still problems to reach convergence due to rough and fragmented surface of the ice deposit. But the author is confident to approximate the ice surface sufficiently smooth in further steps to represent the surface adequately. However, the presented simulation

scheme allows for automatic domain assignment where the number and shape of the bodies under investigation are not known in advance. The model provides the structure to simulate rime ice accretion on conductor bundles can incorporate the physical aspects of glaze and wet snow accretion in the on going research. Before reliable results can be achieved the model needs to be verified by comparison with experimental data. Consequently conclusions on the rime ice development of bundled conductors are expected, based on the assumption of dry growing conditions. The application of conductor bundles, which usually have cables with a diameter of 2 to 4 cm and a spacing of 40 cm, rise the question how the cable in the weak is affected by the up stream cable. Beside qualitative statements form meteorological reports, to the author's knowledge there are no publications on the effect on ice evolution on cylinders in a tandem arrangement. Especially when the icing enlarges the cross section dimensions, an impact on the cable in the weak is expected. Since the ratio of the cable spacing to the characteristic length of the iced cross-section can decrease from about 10 to 5 or less. This would anticipate a chance in the icing particle flux on the cable in the weak.

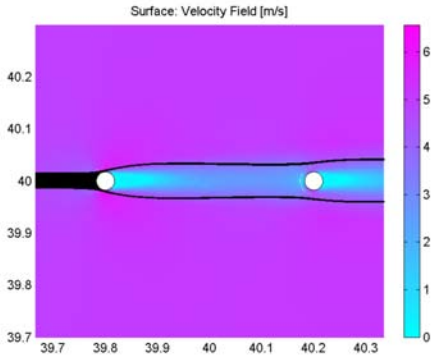

Figure 3: Particle trajectories with a wind velocity of $5m/s$ and a medium volume diameter of $34\mu m$

The figure 3 is showing the shielding effect of the up stream cable on the cable in the weak and figure 4 shows the droplets impinging on the up stream cable.

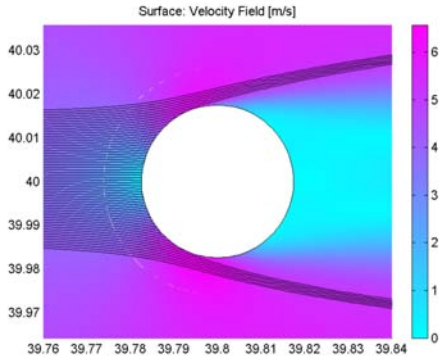

Figure 4: Particle trajectories at the up stream cable with a wind velocity of $5m/s$ and a medium volume diameter of $34\mu m$

References

[1] M Bain and J. F. Gayet, *Contribution to the modeling of the ice accretion process: Ice density variation with the impact surface angle*, Annals of Glaciology **4** (1982), 19–23.

[2] W. B. Bendel and D. Paton, *A review on the effect of ice storms on the power industry*, Journal of Applied Meteorology **20** (1981), 1445–1449.

[3] COMSOL, *Comsol 3.4 chemical engineering module user's guid*, 2007.

[4] J. H. Ferziger and P. Milovan, *Numerische Strömungsmechanik*, Springer-Verlag Berlin Heidelberg, 2008.

[5] J. Franke, *Introduction to the prediction of wind effects on buildings by computational wind engineering (cwe).*

[6] Ping Fu, Masoud Farzaneh, and Gilles Bouchard, *Two-dimensional modelling of the ice accretion process on transmission line wires and conductors*, Cold Regions Science and Technology **46** (2006), 132–146.

[7] Bundesnetzagentur für Elektrizität, Gas, Telekommunikation, Post und Eisenbahnen, *Untersuchungsbericht über die Versorgungsstörung im Netzgebiet des RWE im Münsterland vom 25.11.2005*, 2006.

[8] K. F. Jones, *An evaluation of the severity of the january 1998 ice storm in*

northern new england, Tech. report, Report for FEMA Region 1, 1998.

[9] ———, *A simple model for freezing rain ice loads*, Atmospheric Research **46** (1998), 87–97.

[10] K. F. Jones, J. E. Friddell, S. F. Daly, and C. M. Vuyovich, *Severe winter weather in the continental u.s. and global climate cycles*, Tech. report, ERDC/CRREL TR-04-19, 2004.

[11] D. Lämpke, *Schadensanalyse an im Münsterland umgebrochenen Strommasten*, Tech. report, Bundesanstalt für Materialforschung und Materialprüfung, 2006.

[12] A. Llinca, F. Llinca, and I. Ignat, *Numerical study of iced conductors aerodynamics*, 7th International Workshop on Atmospheric Icing of Structures, 1996.

[13] E. P. Lozowski, J. R. Stallabrass, and P. F. Hearty, *The icing of an unheated nonrotating cylinder. part i: A simulation model*, Journal of Climate and Applied Meteorology **22** (1983), 2053–2074.

[14] W. C. Macklin, *The density and structure of ice formed by accretion*, Quarterly Journal of the Royal Meteorological Society **88** (1962), 30–50.

[15] L. Makkonen, *Modelling of ice accretion on wires*, Journal of Climate and Applied Meteorology **23** (1984), 929–939.

[16] ———, *Models for the growth of rime, glaze, icicles and wet snow on structures*, Phil. Trans. R. Soc. London **358** (2000), 2913–2939.

[17] L. Makkonen and P. Lozowski, E., *Fifty years of progress in modelling the acculation of atmospheric ice on power network equipment*, 11th International Workshop on Atmospheric Icing of Structures, 2005.

[18] N. D. Muhlerin, *Atmospheric icing and communication tower failure in the united states*, Cold Regions Science and Technology **27** (1998), 91–104.

[19] G. Poots, *Ice and snow accretion on structures*, Research Studies Press LTD., 1996.

[20] Wikipedia, *Münsterländer Schneechaos*, http://de.wikipedia.org/wiki/M%C3%BCnsterl%C3%A4nder_Schneechaos, 25th August 2008.

[21] D. C. Wilcox, *Turbulance modeling for CFD*, DCW Industries, 1998.

[22] M. Wildhalm, A. Ronzheimer, and J Meyerz, *Lagrangian particle tracking on large unstructured three-dimensional meshes*, 46th AIAA Aerospace Sciences Meeting and Exhibit, Reno, Nevada, USA, vol. AIAA-2008-472, 2008, pp. 1–19.

Acknowledgements

The author wants to thank the the Deutsche Forschungsgemeinschaft (DFG) for the financial support of this research project.